

Single-shot spatial instability and electric control of polariton condensates at room temperatureYing Gao,^{1,2} Xuekai Ma,^{3,4} Xiaokun Zhai,^{1,2} Chunzi Xing,⁵ Meini Gao,⁵ Haitao Dai,⁵ Hao Wu,⁶ Tong Liu,⁶ Yuan Ren,⁶ Xiao Wang ,⁷ Anlian Pan,⁷ Wei Hu,⁴ Stefan Schumacher,^{3,8} and Tingge Gao ^{1,2}¹*Department of Physics, School of Science, Tianjin University, Tianjin 300072, People's Republic of China*²*Institute of Molecular Plus, Tianjin University, Tianjin 300072, People's Republic of China*³*Department of Physics and Center for Optoelectronics and Photonics Paderborn (CeOPP), Universität Paderborn, Warburger Strasse 100, 33098 Paderborn, Germany*⁴*Guangdong Provincial Key Laboratory of Nanophotonic Functional Materials and Devices, South China Normal University, Guangzhou 510631, People's Republic of China*⁵*Tianjin Key Laboratory of Low Dimensional Materials Physics and Preparing Technology, School of Science, Tianjin University, Tianjin 300072, People's Republic of China*⁶*Lab of quantum detection and awareness, Space Engineering University Beijing 101416, People's Republic of China*⁷*College of Materials Science and Engineering, Hunan University, Changsha 410082, People's Republic of China*⁸*Wyant College of Optical Sciences, University of Arizona, Tucson, Arizona 85721, USA*

(Received 2 May 2023; revised 24 October 2023; accepted 24 October 2023; published 9 November 2023)

In planar microcavities, the transverse-electric and transverse-magnetic (TE-TM) mode splitting of cavity photons can result in optical spin-orbit coupling (SOC). In this work, we find that in a liquid crystal (LC) microcavity filled with perovskite microplates, the pronounced TE-TM splitting gives rise to a strong SOC that leads to the spatial instability of microcavity polariton condensates under single-shot excitation. Spatially varying hole burning occurs between polarization components leading to different condensate profiles from shot to shot. The single-shot polariton condensates become stable when the SOC vanishes as the TE and TM modes are spectrally well separated from each other, which can be achieved by application of an electric field to our LC microcavity with electrically tunable anisotropy. Our findings are well reproduced and traced back to their physical origin by our detailed numerical simulations. With the electrical manipulation our work reveals how the shot-to-shot spatial instability of spatial polariton profiles can be engineered in anisotropic microcavities at room temperature, which will benefit the development of stable polariton-based optoelectronic and light-emitting devices.

DOI: [10.1103/PhysRevB.108.205303](https://doi.org/10.1103/PhysRevB.108.205303)**I. INTRODUCTION**

Mode instability has been reported in different systems resulting from various physical properties, such as the transverse mode instability in laser physics [1,2], modulational instability in nonlinear optics [3], and atomic condensates [4], as well as dynamical instability in hybrid exciton polariton condensates [5]. Exciton polaritons are created when strong coupling between excitons and cavity photon modes in microcavities occurs. Being a composite boson, below the Mott density, exciton polaritons can experience a similar bosonic condensation as cold atoms [6,7], and the polariton condensation can be observed at much higher temperature even up to room temperature [8–10]. Usually the polariton lifetime is very short such that the exciton polariton is a nonequilibrium system. Better thermalization can be realized in a high-Q microcavity where the polariton lifetime can reach hundreds of picoseconds [11]. Under nonresonant pumping, an exciton reservoir can be excited and acts as a source for the polariton condensate; the interaction between the exciton reservoir and the condensate plays a critical role in the condensation process [12–14]. The nonequilibrium nature and the nonlinear interaction between the polaritons and the exciton reservoir can lead to the instability of polariton condensates,

forming phase defects [15,16], filamentation patterns [5,17], or inhomogeneous density distribution in a microwire microcavity [18]. For example, in organic microcavities, the polariton condensate shows shot-to-shot fluctuation under a large pumping spot, while it transforms into nearly uniform spatial distribution when the excitation spot size is decreased [5]. In GaAs based microcavities, the polariton condensate under single-shot excitations shows that its stability against filamentation is very sensitive to the energy relaxation rate and the detuning, which are closely related to the polariton and exciton reservoir interaction [17]. By reversing the effective mass of the polaritons, instable distribution in the 1D microcavity can be tuned to be stable [18]. It is known that the TE-TM splitting can appear within microcavities [19,20]. In the spinor formalism, the TE-TM splitting acts as an effective magnetic field, which influences the distribution of different spin polarized polaritons and results in the optical spin Hall effect [21,22] and the directional flow of polaritons or periodic oscillation of the pseudospin [23–25]. Under large uniform pumping, the spin-orbit coupling (SOC) induced by the resonant oppositely linearly polarized polariton modes leads to unbalanced interaction with the exciton reservoir for different spin components, thus the polariton condensate distribution in the real space can be modified significantly. The previous

works regarding the instability of the polariton condensates only focus on the polaritons condensing in a single branch, that is, the intrinsic SOC induced by two polariton modes as well as the polarization properties are not explicitly considered. How the polariton stability is affected by the induced SOC when different polarized modes are brought into resonance remains unexplored. Typically, the SOC in a given sample is an intrinsic property and cannot be easily manipulated during the measurements.

Liquid crystal (LC) molecule based microcavities offer a platform to electrically control the linearly polarized cavity photon modes [26] as well as the polariton modes [27]. The voltage applied to the microcavity rotates the LC molecule's director orientation, thus the horizontally linearly polarized polariton modes can be tuned whereas the vertically linearly polarized polariton modes are unaffected. The electrical manner to tune the linear polarizations enables the manipulation of the two modes and the resulting SOC. In other words, when the horizontally and vertically linearly polarized modes are near resonant, their energy splitting can cause an effective magnetic field for the generation of the SOC. When the two linear modes are away from each other by applying the voltage onto the microcavity the effective magnetic field vanishes. A tunable optical spin Hall effect has been reported in a LC based optical microcavity [28].

Here, by electrically controlling the polariton modes, we systematically analyze how the SOC influences the stability of the polariton condensate. The stable polariton condensate is observed at 0 V, where the two linear polarizations are completely separated without SOC and the condensate only occupies one of them. At 2.8 V, the polariton condensate is transformed to a strong shot-to-shot variation structure originating from the SOC under intense femtosecond laser excitation, where the two linear polarizations are brought into resonance and both components are nearly equally occupied. Under a higher voltage of 4.1 V, the two linearly polarized modes are lifted again, such that the polaritons condense only at the vertically linearly polarized branch. As a consequence, the polariton condensate from each single-shot excitation becomes spatially stable again. The experimental observations are well reproduced by our numerical simulations. Our work paves the way to investigate the tunability of the polariton stability against filamentation at room temperature as well as to study the underlying physics of the nonequilibrium state transition between unstable to stable ones.

II. EXPERIMENTAL DETAILS

In the experiments, we use a microcavity with CsPbBr₃ as the gain material [Figs. 1(a)–1(c)], where the details can be found in [27]. The microcavity dispersion is measured using a home-made angle-resolved spectroscopy with a femtosecond laser as the pumping source [LightConversion system, 5700 Hz, 400 nm, spot size 40 μm , see Fig. 1(d)]. Figure 2(b) shows the optical image of the microplate (size: 40 μm , thickness: 147 nm) that has been chosen in this work. As shown in Fig. 2(c), several polariton modes are observed because of the larger cavity length which supports multiple cavity modes. The strong coupling between the excitons in the CsPbBr₃ microplate and the multiple cavity modes creates

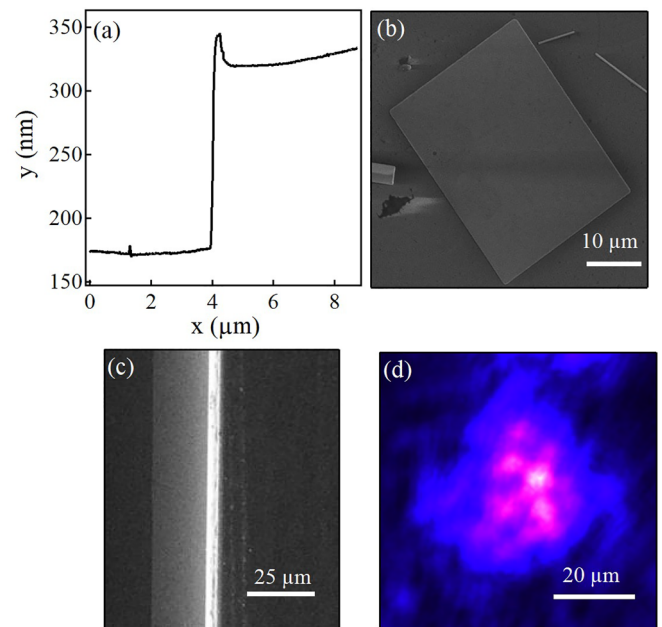


FIG. 1. Basic characterization of the perovskites and the pump spot. (a), (b) Atomic Force Microscope (AFM) and Scanning Electron Microscope (SEM) images of perovskites. (c) SEM cross section image of the liquid crystal microcavity. (d) Pump spot used in the experiment.

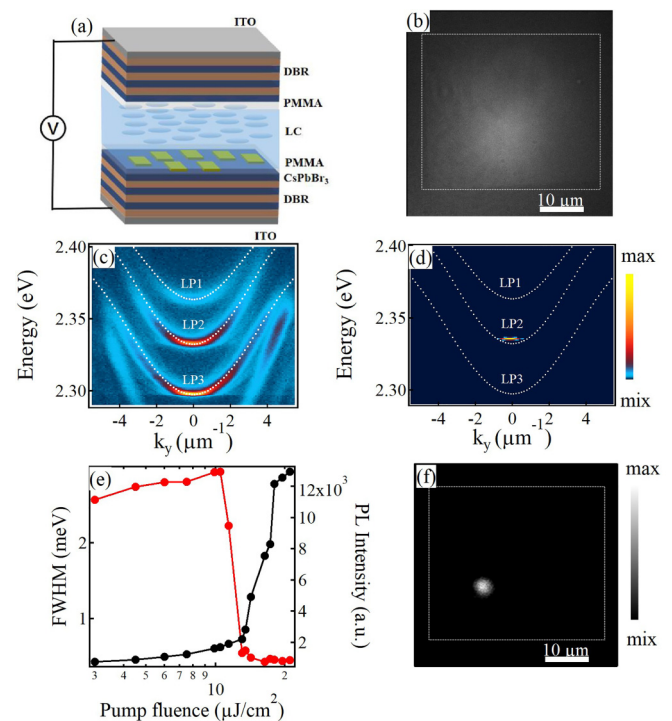


FIG. 2. Exciton polariton condensation in a liquid crystal (LC) microcavity. (a) The microcavity filled with a LC as the cavity spacer layer and with CsPbBr₃ microplates as the gain material. (b) The optical imaging of the perovskite microplate. Photoluminescence dispersion of the microcavity (c) below and (d) above the threshold. The dashed lines are the fitted polariton dispersion. (e) Integrated intensity and linewidth of the polariton against the pumping density. (f) Real space imaging of the polariton condensate under the voltage of 0 V.

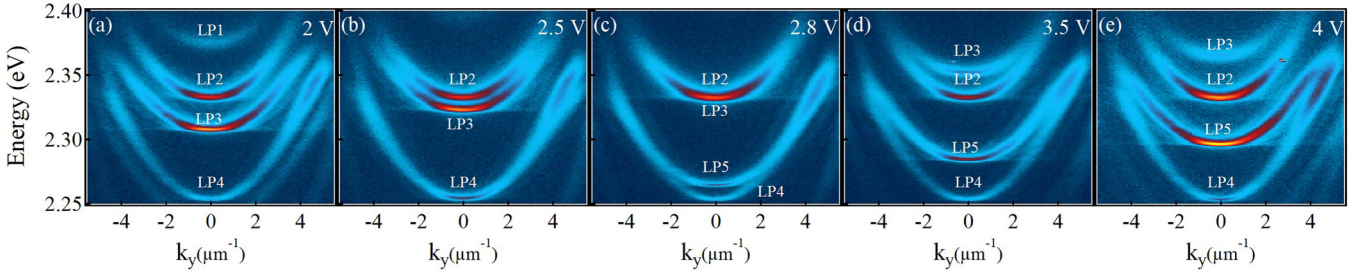


FIG. 3. Photoluminescence dispersion of the microcavity below the threshold at different voltages. (a) 2 V, (b) 2.5 V, (c) 2.8 V, (d) 3.5 V, and (e) 4 V. The continuous tuning of LP3 can be clearly seen against the voltage.

several lower polariton branches LP1-LP3 (other branches are not shown since they do not contribute to the results in this work). The detailed fitting parameters of the polariton modes LP1-LP3 and the corresponding exciton and photon components obtained from the coupled oscillator model are shown in the Supplemental Material [29] for the Hopfield coefficient. Under 0 V, the LC molecule is aligned along the x direction by standard rubbing procedure. The applied electric field rotates the LC molecule director (the perovskites cannot be tilted by the voltage onto the microcavity), so that the horizontally linearly polarized modes LP1 and LP3 can be tuned by increasing the voltage onto the microcavity (the tuning process of the PL dispersion against the voltage is shown in Fig. 3, the reflectivity and transmission data is shown in the Supplemental Material [29]), whereas LP2 is vertically linearly polarized which is immune to the electric field. The linearly polarized dispersion of the microcavity is shown in Fig. 4. Under the pumping density of around $14 \mu\text{J}/\text{cm}^2$, the integrated intensity of the emitted photons from the microcavity under the voltage of 0 V shows obvious superlinear increase against the pumping density, and the linewidth of the polariton mode is greatly reduced, evidencing the occurrence of the polariton condensation at the ground state of the LP2 [see Figs. 2(d) and 2(e)]. In the real space imaging, we observe a Gaussian-shape profile of the condensate [Fig. 2(f)] located in a local area of the microplates due to the inhomogeneity, i.e., disorder, of the sample.

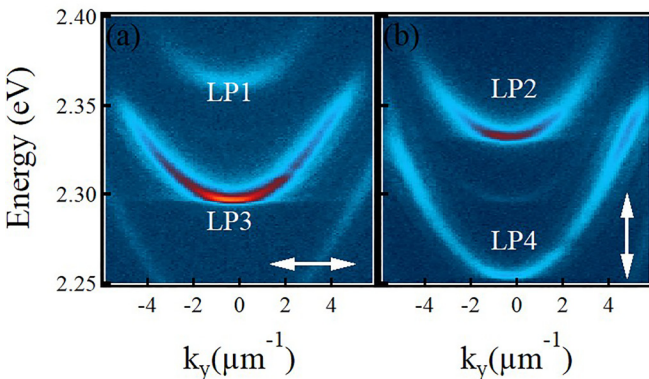


FIG. 4. Photoluminescence dispersion of the microcavity below the threshold. (a) Horizontally and (b) vertically linearly polarized dispersion under the voltage of 0 V.

In the following we perform the single-shot experiments to study the polariton condensate under every pulse excitation. The experimental results with increasing the voltage from 0 V to 4.1 V are shown in Fig. 5 under $1.5 P_{\text{th}}$ and Fig. 6 under $2 P_{\text{th}}$ where the condensed area of polaritons increases. Under 0 V, a stable pattern of the polariton condensate is observed in every single laser pulse excitation (captured by six continuous realizations, of the polariton condensate are plotted in the top panels of Figs. 5 and 6). The variation of the polariton intensity can be neglected for different excitation experiments. Under 0 V, the polaritons mainly condense at LP2 with vertical linear polarization, whereas the population of the horizontally linearly polarized component LP3 can be neglected [see Figs. 7(a) and 7(b)].

III. RESULTS AND DISCUSSIONS

In our microcavity, the field threshold to tune the liquid crystal molecules is smaller (2 V) than the conventional cells [30] due to the large anisotropy of the liquid crystal molecule we used. Increasing the voltage to 2.8 V, the real space imaging of the polariton condensate shows strong shot-to-shot fluctuation, as shown in the middle panels of Figs. 5 and 6. The shot-to-shot fluctuation of the polariton condensate can be observed between the pumping density of $1.5 P_{\text{th}}$ and $2 P_{\text{th}}$ as

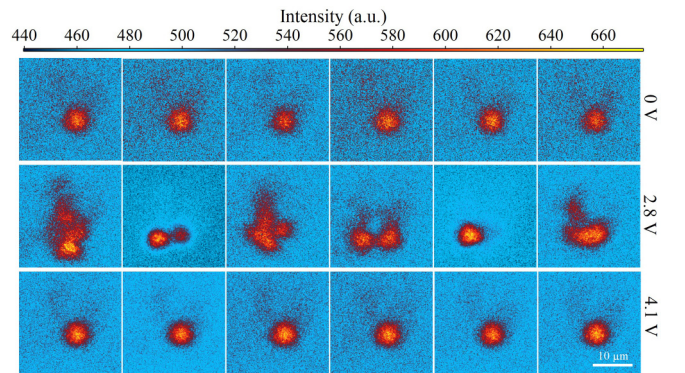


FIG. 5. Single-shot real space imaging of the polariton condensate under different voltages. The top panel, middle panel, and bottom panel correspond to the shot-to-shot spatial polariton condensate distribution taken under the voltage of 0 V, 2.8 V, and 4.1 V, respectively. In each panel, six continuous real space imaging under six laser excitation are shown. The pumping density is fixed at $1.5 P_{\text{th}}$.

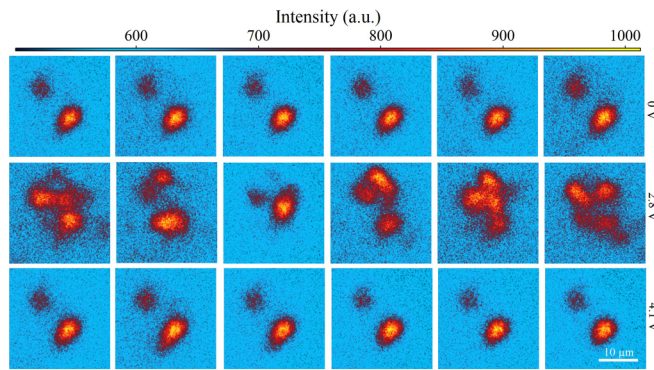


FIG. 6. Single-shot real space imaging of the polariton condensate under different voltages. The top panel, middle panel, and bottom panel correspond to the shot-to-shot spatial polariton condensate distribution taken under the voltage of 0 V, 2.8 V, and 4.1 V, respectively. In each panel, six continuous real space imaging under six laser excitation are shown. The pumping density is fixed at $2 P_{th}$.

the electric field remains unchanged shown in Fig. 6. Similar condensate filamentation have been observed in [5,17]. Especially in GaAs-based microcavities [17], the filamentation of the polariton condensate is determined by the detuning

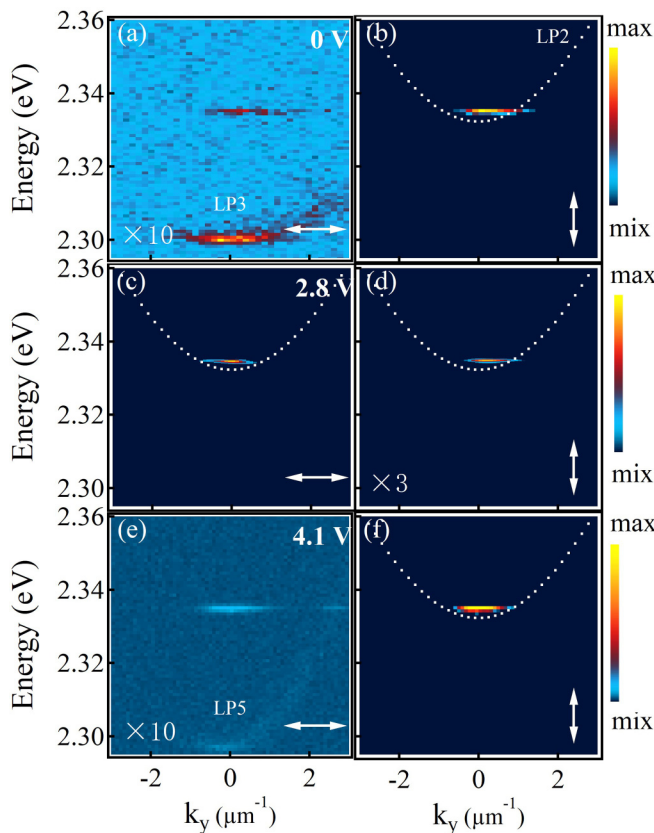


FIG. 7. Linearly polarized dispersion of the polariton condensate. Horizontally and vertically linearly polarized dispersion taken at 0 V (a), (b), 2.8 V (c), (d), and 4.1 V (e), (f). The arrows indicate the polarization directions. (a) and (e) is multiplied by ten, (d) is multiplied by three for the guide of eyes. The horizontal linear polarized modes dominate under the voltage of 0 and 4.1 V.

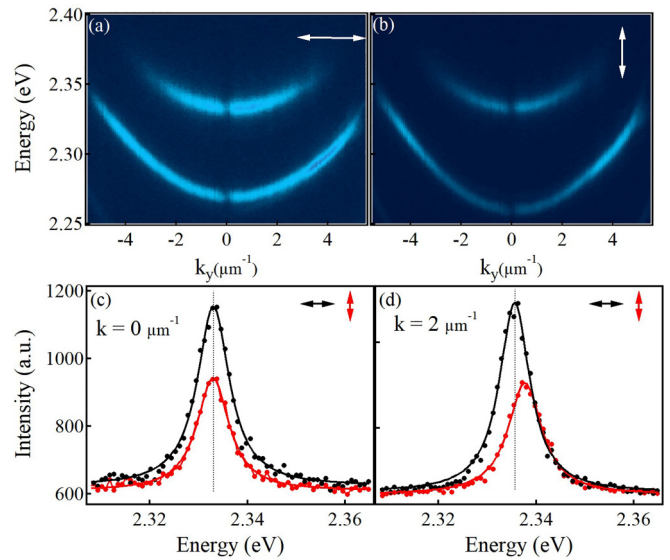


FIG. 8. TE-TM splitting of the microcavity. (a) Horizontally and (b) vertically linearly polarized dispersion of the microcavity. (c) Lineprofile collected at $k_y = 2 \mu\text{m}^{-1}$, indicating that the TE-TM splitting there is around 2.1 meV.

between the excitons and cavity photon modes. When the detuning is negative and the relaxation of the high energy excitons is inefficient, the polariton condensate shows random shot-to-shot fluctuation, which disappears under positive detuning where the polariton-reservoir interaction enhances the condensation process. In our experiments, from Figs. 7(c) and 7(d), one can see that LP3 is tuned to be resonant with LP2 to create a prominent TE-TM splitting (2.1 meV at $2 \mu\text{m}^{-1}$, which is much larger than GaAs microcavities, see Fig. 8), in virtue of the modulation of the XY splitting by the electric field. The strong SOC under the voltage of 2.8 V influences the distribution of polaritons with different spins and thereby the interaction with the exciton reservoir. The resulting unbalance interaction with the exciton reservoir of the two spin components acts as to reshape the condensates differently in each single pulse excitation on set of the condensation process and leads to the random fluctuation of the real space imaging demonstrated by the middle panels of Figs. 5 and 6. We note that the similar single-shot unstable polariton condensate can also be observed in other perovskite microplates in our experiments, which can be seen in the Supplemental Material [29]. Different from GaAs microcavities where the single-shot fluctuation can only be tuned by moving the sample to the area where the detuning is more positive [17] or the instable polariton condensate can become stable by reversing the sign of the mass [18], our work offers a simple method to tune the real space imaging of polariton condensate. In our experiment, when the voltage is larger than 2.8 V, the mode LP3 are tuned to the higher energy, and as a result the polaritons condense mainly to LP2 and show vertical linear polarization [Figs. 7(e) and 7(f)] under the pumping density of $1.5 P_{th}$. In this case, the SOC of the polariton condensate can be ignored. From the real space imaging measurements, one can see that the polariton condensate is stable up to a stronger voltage 4.1 V [see the bottom panels of Figs. 5 and 6].

Generally speaking, as the applied voltage increases from 0 V to 4.1 V, the polariton condensate experiences a stable-unstable-stable gradual process. The two transition states at 2.5 V and 3.4 V, respectively, can be found in the Supplemental Material [29]. The sensitivity of the polariton instability against the voltage in the experiment. In addition, when the pumping density is increased to $2 P_{th}$ under the voltage of 0 V and 4.1 V (Fig. 6), the polariton condensate is still stable although the polariton density at two branches becomes both significant, evidencing that the instability of the polariton condensate under 2.8 V is unrelated to the mode competition or simple mixing between two opposite linear polarization components.

To investigate the principle of the instability observed in our experiments, we mimic the dynamics of polariton condensates by using the binary Gross-Pitaevskii model, i.e., in the circular polarization basis [24],

$$i\hbar \frac{\partial \Psi_{\pm}(\mathbf{r}, t)}{\partial t} = \left[-\frac{\hbar^2}{2m} \nabla_{\perp}^2 - i\hbar \frac{\gamma_c}{2} + g_c |\Psi_{\pm}(\mathbf{r}, t)|^2 + \left(g_r + i\hbar \frac{R}{2} \right) n_{\pm}(\mathbf{r}, t) + V(\mathbf{r}) \right] \Psi_{\pm}(\mathbf{r}, t) + \frac{\Delta_{LT}}{k_{LT}^2} \left(i \frac{\partial}{\partial x} \pm \frac{\partial}{\partial y} \right)^2 \Psi_{\mp}(\mathbf{r}, t). \quad (1)$$

Here, $\Psi_{\pm}(\mathbf{r}, t)$ is the wave function of the polariton condensate and the subscripts \pm denote the spin components. m is the effective mass of the polariton condensate. γ_c is the loss rate in quasimode approximation [31] which can be compensated by the gain from the exciton reservoir $n_{\pm}(\mathbf{r}, t)$ with a condensation rate R . g_c and g_r are the polariton-polariton interaction and polariton-reservoir interaction, respectively. $V(\mathbf{r})$ is the disorder potential with the correlation length $\sim 5 \mu\text{m}$ and the depth $\sim 0.5 \text{ meV}$, representing the rugged sample surfaces, to approximate the experimental condition. Δ_{LT} is the TE-TM splitting at a finite momentum k_{LT} . It is worth pointing out that in our case we assume that the incoherent exciton reservoir $n_{\pm}(\mathbf{r}, t)$ is reshaped by both spin components, because during the condensation process the phase and polarization information of the ‘‘hot’’ excitations are not preserved. Therefore, the equation of motion for the exciton reservoir satisfies

$$\frac{\partial n_{\pm}(\mathbf{r}, t)}{\partial t} = \left[-\gamma_r - \frac{R}{2} (|\Psi_{\pm}(\mathbf{r}, t)|^2 + |\Psi_{\mp}(\mathbf{r}, t)|^2) \right] \times n_{\pm}(\mathbf{r}, t) + P_{\pm}(\mathbf{r}, t). \quad (2)$$

Here, $n_{\pm}(\mathbf{r}, t)$ is the density of the reservoir. γ_r is the loss rate of the reservoir. $P_{\pm}(\mathbf{r}, t)$ is the incoherent and pulsed pump with a standard Gaussian distribution in both real space (diameter $\sim 20 \mu\text{m}$) and time (duration $\sim 50 \text{ ps}$), nonresonantly driving the system for the creation of the polariton condensates. Here we consider a linearly polarized pump with $P_+ = P_-$, which satisfies

$$P_{\pm}(x, y, t) = P_0 e^{-\frac{x^2+y^2}{w_p^2}} e^{-\frac{(t-t_0)^2}{w_t^2}}. \quad (3)$$

Here, $P_0 = 80 \text{ ps}^{-1} \mu\text{m}^{-2}$ is the intensity of the pump, $w_p = 20 \mu\text{m}$ indicates the size of the pump, and $w_t = 50 \text{ ps}$ represents the duration of the pulse which is centered at $t_0 = 20 \text{ ps}$.

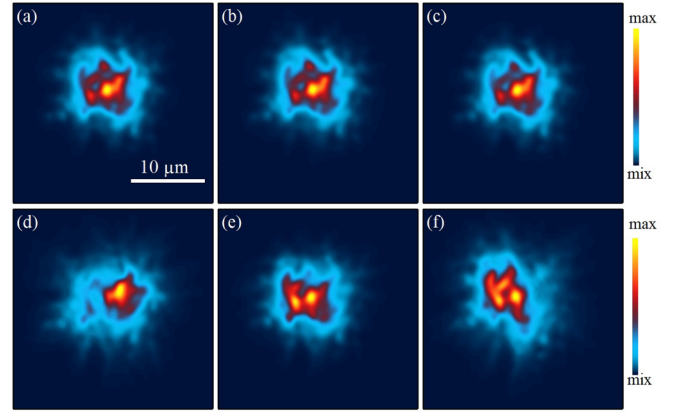


FIG. 9. Numerical results of the single-shot excitation. Time-integrated polariton densities (linearly x -polarized component, i.e., $|\Psi_+ + \Psi_-|^2$) for three single-shot excitations at (a)–(c) $\Delta_{LT} = 0$ in which the solutions are almost identical and (d)–(f) $\Delta_{LT} = 1 \text{ meV}$ where the solutions are distinct. Other parameters for numerical simulations are: $m = 0.2 m_e$ (m_e is the free electron mass), $\gamma_c = 0.2 \text{ ps}^{-1}$, $\gamma_r = 1.5\gamma_c$, $R = 0.03 \text{ ps}^{-1} \mu\text{m}^2$, $g_c = 0.6 \mu\text{eV} \mu\text{m}^2$, $g_r = 2g_c$, and $k_{LT} = 2 \mu\text{m}^{-1}$.

In the above model, the static electric field or its direct influence on the dynamics of polariton condensates is not included. However, from the experimental results, one can see that the two linearly polarized cavity modes can be brought into resonant at around 2.8 V where a clear TE-TM splitting, $\sim 2.1 \text{ meV}$ at $k = 2 \mu\text{m}^{-1}$, is measured (see Fig. 8). This energy splitting, which vanishes when the two modes are completely separated at other voltages, gives rise to a strong SOC, corresponding to the last term on the right side of Eq. (1). From the numerical results, one can see that without SOC, i.e., $\Delta_{LT} = 0$, the distribution of the condensate at each independent excitation is almost identical [Fig. 9(a)–9(c)], while the situation changes when the SOC become significant as shown in Fig. 9(d)–9(f) in which each identical pump pulse creates a different density pattern (from initial noise). This is because the SOC induces different density distributions of the two spin components, such that their contributions to the reshaping of the reservoir are distinct. The reshaped reservoir enables the polaritons to condense in the adjacent local energy minima in the disorder. The numerical results are nicely consistent with the experimental observations shown in Figs. 5 and 6, demonstrating that the instability originates from the strong SOC. The density profiles in Fig. 9 are linearly x polarized, i.e., $|\Psi_+ + \Psi_-|^2$. Every density profile obtained in the numerical simulation is integrated over the entire simulation period ($\sim 100 \text{ ps}$), and in each single-shot excitation a different initial noise condition is applied. Note that the TE-TM splitting used in the numerical simulation is 1 meV at $k_{LT} = 2 \mu\text{m}^{-1}$ which is smaller than that measured in the experiment. The reason for the disagreement between the experiment and theory is that the linewidth of the polariton modes below the threshold measured in the experiment is broad, such that this value may be overestimated.

In our work, one can see that the polaritons condense in the ground state of LP2 and LP3 under the voltage of 2.8 V [Figs. 7(c) and 7(d)], hence the shot-to-shot fluctuation does

not originate from the random transition between the discrete energy levels. This excludes the possibility of the appearance of the transverse mode instability induced long-time random fluctuation resulted from heating effect or quasiperiodic modulation of the refractive index in the fiber lasers [1] (note that the pumping power we used is only $1.5 P_{th}$). In addition, the polariton condensate distribution can be tuned from unstable to stable without changing the detuning [17]. Moreover, comparing with the modulational instability in nonlinear systems which may become stable when the input power is changed, the instability we observed can be engineered to be stable by simply tuning the voltage onto the neutral polaritons in the microcavity.

IV. CONCLUSIONS

To summarize, we have experimentally and theoretically studied how to electrically tune the spatial distribution stability of the polariton condensate in a LC microcavity. In

such systems, the instability of the polariton condensates is due to the strong SOC which occurs when the two linearly polarized polariton modes are brought into resonance by an electric field. As the two linear modes are spectrally separated from each other, the SOC disappears, resulting in the stable polariton condensation. The electrical manipulation of the polariton condensates studied in our work offers to develop stable polariton-based optoelectronic devices and circuits.

ACKNOWLEDGMENTS

T.G. acknowledges the support from the National Natural Science Foundation of China (NSFC) (No. 12174285), H.D. appreciates the support from the NSFC (No. 61975748), W.H. and Y.R. thank the NSFC (No. 62203466 and No. 62173342, respectively), X.W. appreciates the NSFC (52022029), and the Paderborn group acknowledges the support from the Deutsche Forschungsgemeinschaft (DFG) (Grants No. 467358803 and No. 519608013).

-
- [1] C. Jauregui, C. Stihler, and J. Limpert, Transverse mode instability, *Adv. Opt. Photon.* **12**, 429 (2020).
- [2] C. Jauregui, J. Limpert, and A. Tünnermann, High-power fibre lasers, *Nat. Photonics* **7**, 861 (2013).
- [3] G. P. Agrawal, Nonlinear fiber optics, in *Nonlinear Science at the Dawn of the 21st Century*, edited by P. L. Christiansen, M. P. Sørensen, and A. C. Scott, Lecture Notes in Physics (Springer, Berlin, Heidelberg, 2000), Vol. 542, pp. 195–211.
- [4] K. Strecker, G. Partridge, A. Truscott, and R. Hulet, Formation and propagation of matter-wave soliton trains, *Nature (London)* **417**, 150 (2002).
- [5] N. Bobrovska, M. Matuszewski, K. S. Daskalakis, S. A. Maier, and S. Kéna-Cohen, Dynamical instability of a nonequilibrium exciton-polariton condensate, *ACS Photonics* **5**, 111 (2018).
- [6] J. Kasprzak, M. Richard, S. Kundermann, A. Baas, P. Jembrun, J. M. J. Keeling, F. M. Marchetti, M. H. Szymańska, R. André, J. L. Staehli, V. Savona, P. B. Littlewood, B. Deveaud, and L. S. Dang, Bose-Einstein condensation of exciton polaritons, *Nature (London)* **443**, 409 (2006).
- [7] R. Balili, V. Hartwell, D. Snoke, L. Pfeiffer, and K. West, Bose-Einstein condensation of microcavity polaritons in a trap, *Science* **316**, 1007 (2007).
- [8] S. Christopoulos, G. Baldassarri Höger von Högersthal, A. J. D. Grundy, P. G. Lagoudakis, A. V. Kavokin, J. J. Baumberg, G. Christmann, R. Butté, E. Feltn, J. F. Carlin, and N. Grandjean, Room-temperature polariton lasing in semiconductor microcavities, *Phys. Rev. Lett.* **98**, 126405 (2007).
- [9] K. S. Daskalakis, S. A. Maier, R. Murray, and S. Kéna-Cohen, Nonlinear interactions in an organic polariton condensate, *Nat. Mater.* **13**, 271 (2014).
- [10] J. D. Plumhof, T. Stöferle, L. J. Mai, U. Scherf, and R. F. Mahrt, Room-temperature Bose-Einstein condensation of cavity exciton-polaritons in a polymer, *Nat. Mater.* **13**, 247 (2014).
- [11] Y. Sun, P. Wen, Y. Yoon, G. Liu, M. Steger, L. N. Pfeiffer, K. West, D. W. Snoke, and K. A. Nelson, Bose-Einstein condensation of long-lifetime polaritons in thermal equilibrium, *Phys. Rev. Lett.* **118**, 016602 (2017).
- [12] M. Wouters and V. Savona, Stochastic classical field model for polariton condensates, *Phys. Rev. B* **79**, 165302 (2009).
- [13] F. Tassone, C. Piermarocchi, V. Savona, A. Quattropani, and P. Schwendimann, Bottleneck effects in the relaxation and photoluminescence of microcavity polariton, *Phys. Rev. B* **56**, 7554 (1997).
- [14] D. D. Solnyshkov, H. Terças, K. Dini, and G. Malpuech, Hybrid Boltzmann-Gross-Pitaevskii theory of Bose Einstein condensation and superfluidity in open driven-dissipative systems, *Phys. Rev. A* **89**, 033626 (2014).
- [15] J. Keeling and N. G. Berloff, Spontaneous rotating vortex lattices in a pumped decaying condensate, *Phys. Rev. Lett.* **100**, 250401 (2008).
- [16] T. C. H. Liew, O. A. Egorov, M. Matuszewski, O. Kyriienko, X. Ma, and E. A. Ostrovskaya, Instability-induced formation and nonequilibrium dynamics of phase defects in polariton condensates, *Phys. Rev. B* **91**, 085413 (2015).
- [17] E. Estrecho, T. Gao, N. Bobrovska, M. D. Fraser, M. Steger, L. Pfeiffer, K. West, T. C. H. Liew, M. Matuszewski, D. W. Snoke, A. G. Truscott, and E. A. Ostrovskaya, Single-shot condensation of exciton polaritons and the hole burning effect, *Nat. Commun.* **9**, 2944 (2018).
- [18] F. Baboux, D. De Bernardis, V. Goblot, V. N. Gladilin, C. Gomez, E. Galopin, L. Le Gratiet, A. Lemaître, I. Sagnes, I. Carusotto, M. Wouters, A. Amo, and J. Bloch, Unstable and stable regimes of polariton condensation, *Optica* **5**, 1163 (2018).
- [19] Y. Gao, Y. Li, X. K. Ma, M. N. Gao, H. T. Dai, S. Schumacher, and T. G. Gao, Tilting nondispersive bands in an empty microcavity, *Appl. Phys. Lett.* **121**, 201103 (2022).
- [20] I. A. Shelykh, A. V. Kavokin, Y. G. Rubo, T. C. H. Liew, and G. Malpuech, Polariton polarization-sensitive phenomena in planar semiconductor microcavities, *Semicond. Sci. Technol.* **25**, 013001 (2010).
- [21] A. Kavokin, G. Malpuech, and M. Glazov, Optical spin Hall effect, *Phys. Rev. Lett.* **95**, 136601 (2005).

- [22] H. Terças, H. Flayac, D. D. Solnyshkov, and G. Malpuech, Non-abelian gauge fields in photonic cavities and photonic superfluids, *Phys. Rev. Lett.* **112**, 066402 (2014).
- [23] C. Leyder, M. Romanelli, J. Ph. Karr, E. Giacobino, T. C. H. Liew, M. M. Glazov, A. V. Kavokin, G. Malpuech, and A. Bramati, Observation of the optical spin Hall effect, *Nat. Phys.* **3**, 628 (2007).
- [24] E. Kammann, T. C. H. Liew, H. Ohadi, P. Cilibrizzi, P. Tsotsis, Z. Hatzopoulos, P. G. Savvidis, A. V. Kavokin, and P. G. Lagoudakis, Nonlinear optical spin Hall effect and long-range spin transport in polariton lasers, *Phys. Rev. Lett.* **109**, 036404 (2012).
- [25] X. Ma, Y. V. Kartasho, A. Kavokin, and S. Schumacher, Chiral condensates in a polariton hexagonal ring, *Opt. Lett.* **45**, 5700 (2020).
- [26] K. Rechcińska, M. Król, R. Mazur, P. Morawiak, R. Mirek, K. Łempicka, W. Bardyszewski, M. Matuszewski, P. Kula, W. Piecek, P. G. Lagoudakis, B. Piętka, and J. Szczytko, Engineering spin-orbit synthetic Hamiltonians in liquid-crystal optical cavities, *Science* **366**, 727 (2019).
- [27] Y. Li, X. Ma, X. K. Zhai, M. N. Gao, H. T. Dai, S. Schumacher, and T. G. Gao, Manipulating polariton condensates by Rashba-Dresselhaus coupling at room temperature, *Nat. Commun.* **13**, 3785 (2022).
- [28] K. Lekenta, M. Król, R. Mirek, K. Łempicka, D. Stephan, R. Mazur, P. Morawiak, P. Kula, W. Piecek, P. G. Lagoudakis, B. Piętka, and J. Szczytko, Tunable optical spin Hall effect in a liquid crystal microcavity, *Light Sci. Appl.* **7**, 74 (2018).
- [29] See Supplemental Material at <http://link.aps.org/supplemental/10.1103/PhysRevB.108.205303> for the voltage dependent reflectivity, transmission and Hopfield coefficient, the single shot real space imaging under other voltage, and another perovskite.
- [30] O. Masahito and K. Katsumi, Electro-optical characteristics and switching behavior of the in-plane switching mode, *Appl. Phys. Lett.* **67**, 25 (1995).
- [31] M. Carcamo, S. Schumacher, and R. Binder, Transfer function replacement of phenomenological single-mode equations in semiconductor microcavity modeling, *Appl. Opt.* **59**, G112 (2020).